Simple and Versatile Platforms for Manipulating Light with Matter: Strong Light–Matter Coupling in Fully Solution-Processed Optical Microcavities

Andrew Strang, Victoria Quirós-Cordero, Pascal Grégoire, Sara Pla, Fernando Fernández-Lázaro, Ángela Sastre-Santos, Carlos Silva-Acuña,* Paul N. Stavrinou,* and Natalie Stingelin*

Planar microcavities with strong light–matter coupling, monolithically processed fully from solution, consisting of two polymer-based distributed Bragg reflectors (DBRs) comprising alternating layers of a high-refractive-index titanium oxide hydrate/poly(vinyl alcohol) hybrid material and a low-refractive-index fluorinated polymer are presented. The DBRs enclose a perylene diimide derivative (b-PDI-1) film positioned at the antinode of the optical mode. Strong light–matter coupling is achieved in these structures at the target excitation of the b-PDI-1. Indeed, the energy-dispersion relation (energy vs in-plane wavevector or output angle) in reflectance and the group delay of transmitted light in the microcavities show a clear anti-crossing—an energy gap between two distinct exciton-polariton dispersion branches. The agreement between classical electrodynamic simulations of the microcavity response and the experimental data demonstrates that the entire microcavity stack can be controllably produced as designed. Promisingly, the refractive index of the inorganic/organic hybrid layers used in the microcavity DBRs can be precisely manipulated between values of 1.50 to 2.10. Hence, microcavities with a wide spectral range of optical modes might be designed and produced with straightforward coating methodologies, enabling fine-tuning of the energy and lifetime of the microcavities' optical modes to harness strong light–matter coupling in a wide variety of solution processable active materials.

1. Introduction

Strong light–matter coupling between quantized modes of the electromagnetic field (optical modes) and excitonic transitions of an active material give rise to exciton-polaritons.[1–5] Exciton-polaritons are hybrid quasiparticles that feature properties from both their light and matter constituents, including a low effective mass compared to bare excitons due to the "light" component as well as many-body interactions governed by the "exciton" component. Such hybrid light–matter states are interesting as they can provide energetic pathways that alter photophysical processes involved in, e.g., light emission;[6–10] they may also form exotic quantum phases of matter that display macroscopic coherence at room temperature, so-called Bose–Einstein condensates,[11–17] which lead to highly correlated behavior such as superfluidity.[18] In addition, control of polaritons via microcavity design might be exploited for elongating the lifetime of molecular transitions and excited states[19]—which could result in new

A. Strang
Department of Physics and Centre for Plastic Electronics
Imperial College London
London SW7 2AZ, UK

V. Quirós-Cordero, N. Stingelin
School of Materials Science and Engineering
Georgia Institute of Technology
Atlanta, Georgia 30332, USA
E-mail: natalie.stingelin@gatech.edu

P. Grégoire
Département de Physique et Regroupement Québécois sur les Matériaux de Pointe
Université de Montréal
Case Postale 6128, succursale Centre-ville, Montréal H3C 3J7, Canada

S. Pla, F. Fernández-Lázaro, Á. Sastre-Santos
Área de Química Orgánica
Instituto de Bioingeniería
Universidad Miguel Hernández
Elche 03202, Spain

C. Silva-Acuña
School of Physics and School of Chemistry and Biochemistry
Georgia Institute of Technology
Atlanta, Georgia 30332, USA
E-mail: carlos.silva@gatech.edu

P. N. Stavrinou
Information Engineering Building
Department of Engineering Science
University of Oxford
9 Parks Road, Oxford OX1 3PD, UK
E-mail: paulstavrinou@eng.ox.ac.uk

N. Stingelin
School Chemical and Biochemical Engineering
Georgia Institute of Technology
Atlanta, Georgia 30332, USA

reaction pathways and open the possibility of tailoring chemical reactivity rates.[20]

To date, metallic mirrors or inorganic DBRs have been typically used to fabricate optical microcavities confining an optical mode.[21] This frequently limits the choice of the spacer-layer material(s) since thermal deposition or sputtering of the top mirror can negatively affect the underlying stack, including the active light-absorbing/light-emitting excitonic material. For example, a previous study showed that the deposition of the top Ta_2O_5/SiO_2 DBR via electron beam and reactive thermal evaporation, respectively, can lead to the cracking of the active material film.[22] Alternatively, optical microcavities may be realized by first producing the mirrors and then, in a second step, filling the gap between them with an active material.[16,23,24] For organic active materials, solution- or melt-processing can be used for the filling step, but achieving high-quality interfaces between the active layer and the mirror structures can be challenging. Having the capability to produce structures fully from solution with little—if any—effect on the spacer layers, would enable the use of a wider range of materials for the absorbing/emissive species (e.g., organic dyes, polymers, quantum dots dispersed in polymer matrices, etc.). We set out here to demonstrate the successful fabrication of planar microcavities, processed entirely from solution at ambient conditions. The microcavities are designed and fabricated in a highly precise manner to spectrally align an optical mode in near-resonance with the 0-0 vibronic transition of a model organic semiconductor, a perylene diimide derivative (*b*-PDI-1),[25] leading to strong light–matter coupling. The key is the use of a versatile inorganic/organic molecular hybrid material that can be designed to display a high refractive index, leading to a high-refractive-index contrast when combined with a low-refractive-index polymer.[26,27] Because of its amorphous nature (see refs. [26–28]), moreover, this hybrid material features a very low optical loss and can be readily processed into high-quality films (see Figure S1, Supporting Information).[26,27] This allows straightforward fabrication of DBR/spacer-layers/DBR microcavities in a monolithic-like fashion, i.e., layer by layer, obviating the need to fill the cavity region after fabrication. The approach further permits using sensitive materials as the active layer, including high-temperature-sensitive matter.

2. Results and Discussions

We started to explore the potential to produce high-quality optical cavities fully from solution using dip-coating as the deposition method and selecting for the fabrication of the DBRs a high-refractive-index titanium oxide hydrate/poly(vinyl alcohol) (PVAl) molecular hybrid system, a material for which the refractive index can be readily modulated between 1.50 and 2.10.[26–28] We focused on a hybrid material with 60 vol% titanium oxide hydrate that has been well studied[26–28] and that, after annealing, typically leads to a refractive index $n_{high} = 1.76$ at 1.962 eV, as previously identified from Fabry-Pérot oscillations on a single film[26–28] (see Sections S2 and S5 in the Supporting Information for details). This composition of the inorganic/organic hybrid material was selected because it provides the best tradeoff between a high refractive index, low optical loss, and good film formation, as previously reported in detail in refs. [26–28]. Hybrid materials with lower titanium oxide hydrate content have a lower refractive index, leading to a stopband of lower reflectivity and an optical mode of lower Q-factor (see Section S6 in the Supporting Information). Compositions of higher titanium oxide hydrates content are often more difficult to process and can lead to TiO_2 nanoparticle formation over time, resulting in optical loss. For the low-refractive-index material, a commercially available fluorinated polymer, poly[4,5-difluoro-2,2-bis(trifluoromethyl)-1,3-dioxole-co-tetrafluoroethylene] (PFP), featuring a refractive index $n_{low} = 1.30$ at 1.962 eV,[27] was selected. The chemical structures of these materials are shown in **Figure** 1a, right.

As the first step, using the transfer matrix method (TMM)[29] (fully described in Section S11 in the Supporting Information), we designed a 'passive' optical cavity, i.e., a microcavity with a non-absorptive and non-emissive spacer layer placed between the mirrors, depicted in Figure 1a, left. We targeted a cavity based on two six-bilayer DBRs with the spacer layer made of the same high-refractive-index material used in the DBRs and aimed at producing a normal incident cavity resonance at an energy, $E_{Opt.}$ of 1.962 eV, i.e., ≈632 nm, a common wavelength for active organic materials to display optical transitions.

Input parameters for our TMM calculations include energy-dependent refractive indices for the low-/high-refractive-index DBR materials, as well as the spacer layer (see equation 1 and Table S2 in the Supporting Information). These dispersive relations were confirmed previously for the materials of choice (PFP: for the low-refractive-index layers; annealed 60 vol% titanium oxide hydrate/PVAl hybrid: for the high-refractive-index and spacer layers).[27,28] The DBRs in our microcavities were chosen to satisfy a quarter-wave condition, i.e., $n_{layer}(\lambda_{Opt.}) \times d_{layer} = (\lambda_{Opt.}/4)$, where $\lambda_{Opt.}$ corresponds to the target optical mode wavelength (or energy, $E_{Opt.}$), n_{layer} represents the refractive index of the high- or low-refractive-index DBR layer taken at $\lambda_{Opt.}$, and d_{layer} the respective layer thickness. For the spacer layer separating the two DBRs, we choose a wavelength cavity resonance, i.e., $n_{spacer}(\lambda_{Opt.}) \times d_{spacer} = \lambda_{Opt.}$[30] From these expressions, the required layer thicknesses were: 91 nm (high-refractive-index layer), 120 nm (low-refractive-index layer), and 359 nm (spacer layer).

The entire structure was produced via dip-coating using the selected materials and the calculated layer thicknesses. After producing, layer by layer, the first DBR, starting with a high-refractive-index titanium oxide hydrate/PVAl hybrid layer and ending with a PFP layer, the spacer layer (made of the high-refractive-index molecular hybrid) was coated directly onto the first DBR. Following this, the second DBR was produced similarly, depositing first a low-refractive-index layer onto the spacer and ending on a high-refractive-index layer (see Figure 1a; high-refractive-index layers are given in dark gray, low-refractive-index PFP layers in light gray). As described in refs. [26–28], layer thicknesses may be controlled via the solution viscosity and dip-coating withdrawing speed. Post-deposition control of the refractive index for the hybrid material was achieved via thermal annealing.[26–28] Once produced, the entire passive microcavity was annealed at 150 °C, leading to a $n_{high} = 1.76$ at 1.962 eV while not affecting n_{low}, resulting in a higher refractive-index contrast between the PFP layers and the layers produced with the inorganic/organic hybrid material.[27] (Note: Post-annealing leads to contraction of the high-refractive-index layers—an effect that can
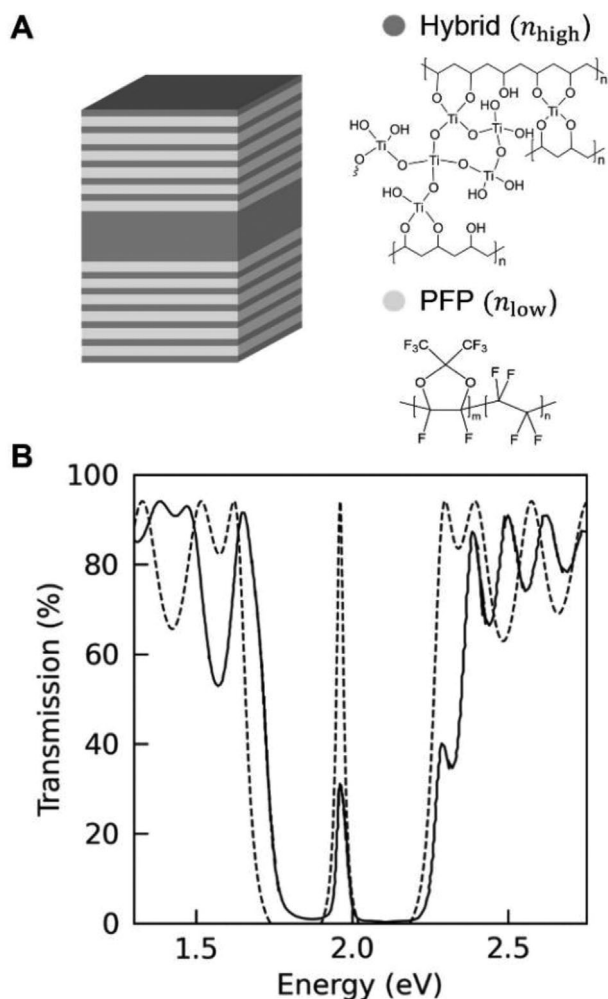
**ADVANCED
SCIENCE NEWS**

www.advancedsciencenews.com

**ADVANCED
MATERIALS**

www.advmat.de

Figure 1. Optical mode of a passive microcavity produced monolithically from solution via dip-coating at ambient conditions. A) Exemplary microcavity, composed of alternating layers of a high-refractive-index 60 vol% titanium oxide hydrate/poly(vinyl alcohol) hybrid material and a low-refractive-index fluoropolymer, PFP. The microcavity consists of two six-bilayer DBRs that are separated by a spacer layer also consisting of the hybrid material. The PFP has a refractive index n_{low} = 1.30 at 1.962 eV; while the refractive index of the annealed titanium oxide hydrate/PVAl material is n_{high} = 1.76 at 1.962 eV. B) Comparison of experimentally measured (solid line) and calculated transmission (dashed line) at normal incidence for such a microcavity. For the transfer matrix calculation, we used the energy-dependent refractive index of, respectively, the low- and the high-refractive-index DBR layers/the high-refractive-index spacer layer, and the following layer thicknesses: 91 nm (high-refractive-index layer), 120 nm (low-refractive-index layer), and 359 nm (spacer layer). The measured optical mode at 1.962 eV shows very good agreement with the calculated microcavity response (dashed line).

be readily accounted for, as verified by TMM calculations and as demonstrated in refs. [26–28]).

Reassuringly, the transmission spectrum for the fully solution-processed passive cavity (Figure 1b, solid line) is in rather good agreement with the TMM calculations (Figure 1b, dashed line). Most importantly, a high-transmission optical mode at the target energy $E_{Opt.}$ of 1.962 eV is observed within the cavity stopband, i.e., the region of low transmission, as desired. This ob-

servation illustrates that straightforward solution processing can lead to high-quality optical microcavities. Indeed, the slight discrepancy between the measured and calculated transmission of the optical mode (i.e., at $E_{Opt.}$ of 1.962 eV) is attributed to the limited spectral resolution of the UV–vis spectrophotometer employed to measure the microcavity's transmission and to spatial variations of the light source's spot size due to vibrations. Small uncertainties associated with the experimental determination of the refractive indices and thicknesses of all layers, used as inputs for the transfer matrix method, can also lead to certain differences between the transmission measurement and calculation. Since transmission electron microscopy (TEM) reveals the excellent quality of the multilayer stacks and their interfaces (see Figure S4, Supporting Information), with essentially negligible interdiffusion between the low and high refractive index materials (Figure S4b, Supporting Information), in agreement with previous reports,[26,27] we do not assign these discrepancies to defects in the multilayer structure.

This view is supported by the fact that the Q-factor, $Q = E_{Opt.}/\Delta_{FWHM}(E_{Opt.})$, of the passive solution-processed cavity is ≈50, which compares relatively well with the value of 71 calculated with TMM simulations. This appears to be a significantly lower value than those reported for most traditional inorganic DBR-DBR and hybrid metal/DBR-DBR microcavities (Q ≈ 100–3000).[13,14,16,17,23,24,31–34] However, these microcavities are typically produced with DBRs of 9–12 bilayers, a significantly higher number of bilayers in comparison to that of our architectures, where we used 4- and 6-bilayer DBRs. We thus expect that, by employing solution-processed DBRs of a larger number of bilayers, we can fabricate microcavities with comparable Q-factors to those obtained with conventional inorganic microcavity structures, as indicated by the TMM simulations included in the (Section S6, Supporting Information). Initial results on individual DBRs produced with a larger number of bilayers are promising. We find that when increasing the number of bilayers in our solution-processed DBRs to 11.5-bilayers, using a 60 vol% titanium oxide hydrate/PVAl hybrid and PFP, and annealing the entire stack at 140 °C (resulting in a n_{high} = 1.79 and n_{low} = 1.29 at 645 nm), the performance of such a DBR is essentially identical to that of a benchmark TiO_2/SiO_2 DBR of a very similar number of layers fabricated by electron-beam deposition (**Figure 2**). Indeed, the stopbands of the two DBRs basically match with respect to both the achieved reflection and stopband width; both, but especially the latter, reflect the quality and magnitude of the refractive-index contrast between layers making up the DBR.

Encouraged by these results, we fabricated a wavelength microcavity based on two four-bilayer DBRs as mirrors, but this time including an active organic semiconductor layer within the spacer (purple layer in the schematic shown in **Figure 3**a, left). We chose b-PDI-1, a perylene diimide derivative, as a model active organic material because such a 1,7-bay-substituted structure provides a high oscillator strength, high quantum yield, small Stokes shift, monomer-like excitations, and low photoluminescence (PL) quenching, even in the solid state, assisted by the low tendency of b-PDI-1 to aggregate. The latter feature is due to the chemical design, through the use of large and complex substituents to limit the close packing of the molecules.[25] The chemical structure of b-PDI-1 is shown in Figure 3a, right.

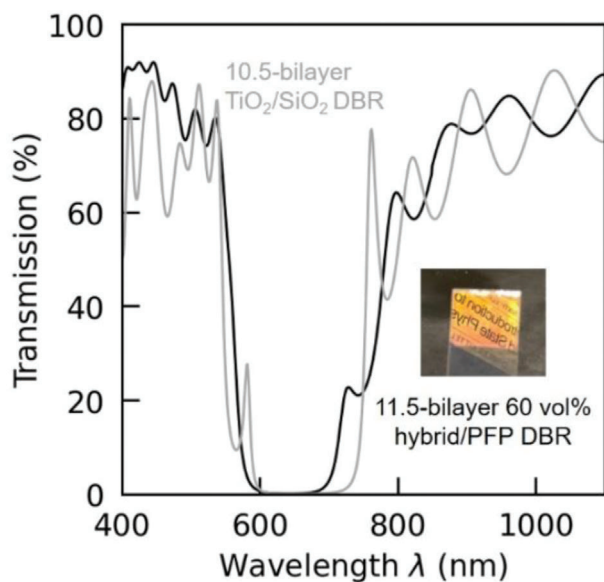**Figure 2.** Comparison between a solution-processed 11.5-bilayer DBR (in black) and a 10.5-bilayer benchmark inorganic DBR fabricated by electron-beam deposition (in gray). Both DBRs display comparable stopband widths as well as near-identical transmission and, consequently, reflection in the stopband. The fabrication of the solution-processed DBR included a final annealing step at 140 °C. A photograph of the solution-processed DBR is presented in the inset, illustrating the high reflectivity that is achieved with such a DBR, enabling mirroring of objects (here: some text) hold above the DBR.

Using the same approach as outlined above for the passive microcavity, we calculated the required layer thicknesses for the cavity region to establish an optical mode with an energy $E_{\text{Opt.}} = 2.112$ eV ($\lambda_{\text{Opt.}} = 587$ nm) at normal incidence ($|\vec{k}_{\parallel}| = 0$) near-resonant with the 0-0 vibronic transition of the semiconductor (Figure 3b). Since the maximum absorption of the exciton appears at $E_{\text{Exc.}} = 2.171$ eV, the idea is to provide a degree of detuning (δ) between the optical mode and the absorption maximum at normal incidence, i.e., $\delta = [E_{\text{Opt.}}(|\vec{k}_{\parallel}| = 0) - E_{\text{Exc.}}] = -59$ meV.

We selected a 30 nm thin, emissive b-PDI-1 spacer layer because this thickness offers the best compromise between film formation, prevention of aggregation, and light absorption. Additional high-refractive-index titanium oxide hydrate/PVAl spacers (see Figure 3a, dark grey layers next to the active film, given in purple) were introduced to fulfill the microcavity wavelength condition and to position the b-PDI-1 film at the antinode of the optical mode's electromagnetic field. This is required to promote light–matter coupling and to prevent the uncoupled exciton response from dominating the microcavity's optical behavior, as observed in previous studies.[35]

Information on light–matter coupling in the active microcavity may be obtained from measuring the microcavity energy dispersion (polariton energy vs in-plane wavevector or output angle) using Fourier microscopy in reflectance.[36] Signatures of strong light–matter coupling can be inferred from this measurement (Figure 3c, top). Two dispersion branches, discerned as diffuse blue halos and distinct from the dispersion of the microcavity's optical mode (dotted blue line; described by $E_{\text{Opt.}}(|\vec{k}_{\parallel}|) = $

$2.112 + 1.347 \times 10^{-3} |\vec{k}_{\parallel}|^2$ eV—see Section S8 in the Supporting Information for specifics on this calculation) and the 0-0 vibronic transition of the b-PDI-1 (dotted purple line), are identified with the upper and lower polariton eigenstates from a Jaynes–Cummings Hamiltonian (black solid lines, overlaid to the measured data; see Figure 3c, top).[37,38] We note that the simulated upper and lower polariton branches (Figure 3c, bottom; blue halos) have slightly higher energies than those measured experimentally. We attribute these minor discrepancies to the uncertainties associated with the experimental inputs, including the refractive indices and thicknesses of each layer. Moreover, for the TMM simulation of the optical mode (Figure 3c, Opt. and Figure S8, Supporting Information), we assigned the active layer a static non-absorptive refractive index value of 1.90, corresponding to its real part at the target optical mode energy of 2.112 eV. For modeling the energy dispersion relation (Figure 3c, bottom), the energy- (i.e., wavelength-) dependent complex refractive index of b-PDI-1 (Figure S2, Supporting Information) was considered.

Significantly, the presented data allows us to quantify the strength of light–matter coupling by deducing a Rabi splitting, Ω, from the anticrossing (i.e., energy gap) between polariton branches at ≈ 6.5 μm^{-1} (20°)—the wavevector (or angle) where the microcavity's optical mode (Figure 3c, Opt.) is resonant with the exciton absorption (Figure 3c, Exc.). We obtain $\Omega = 65$ meV and $\delta = -59$ meV, as expected from our TMM simulations (Figure 3c, bottom). The former agreement provides additional evidence for strong light–matter coupling in our b-PDI-1 cavity, and the latter agreement highlights the accuracy and reliability of our solution-processing approach to design and produce high-quality microcavities confining a desired optical mode; the measured detuning δ agrees nicely with the calculated value when using $E_{\text{Opt.}}(|\vec{k}_{\parallel}| = 0) = 2.112$ eV and $E_{\text{Exc.}} = 2.171$ eV (see above).

The microcavity was further characterized by measuring the spectral phase shift and group delay imparted by the multilayer stack to transmitted light. For this, we propagated a femtosecond pulse train through the multilayer structure and analyzed the effects of the microcavity on the pulse's temporal distortion. To explain this approach, we note that wavepackets—a collection of electromagnetic waves, each with its own frequency and group velocity (propagation velocity through a medium)—describe polychromatic light in classical electrodynamics. As wavepackets propagate through matter, the refractive index $n(\lambda)$ of the propagation medium causes their constituent electromagnetic waves of different frequencies to travel at different velocities, resulting in a phase shift and a group delay (τ_g) that vary with energy. In the absence of strong light–matter coupling, the group delay observed would be governed by the microcavity's optical mode due to the large refractive-index contrast between consecutive alternating layers constituting the microcavity DBRs.[39,40] Additionally, smaller temporal distortions caused by the real part of the active material's refractive index, which displays a dispersive lineshape, could be present. Conversely, in microcavity structures supporting polaritons, further effects on the group delay are expected due to the mixing of light and matter properties.

Effects of such strong light–matter interactions were isolated here by determining the group delay as a function of energy and incident angle (Figure 3d, left; solid lines). Thereby, the phase shift imparted to wavepackets by the microcavity was measured
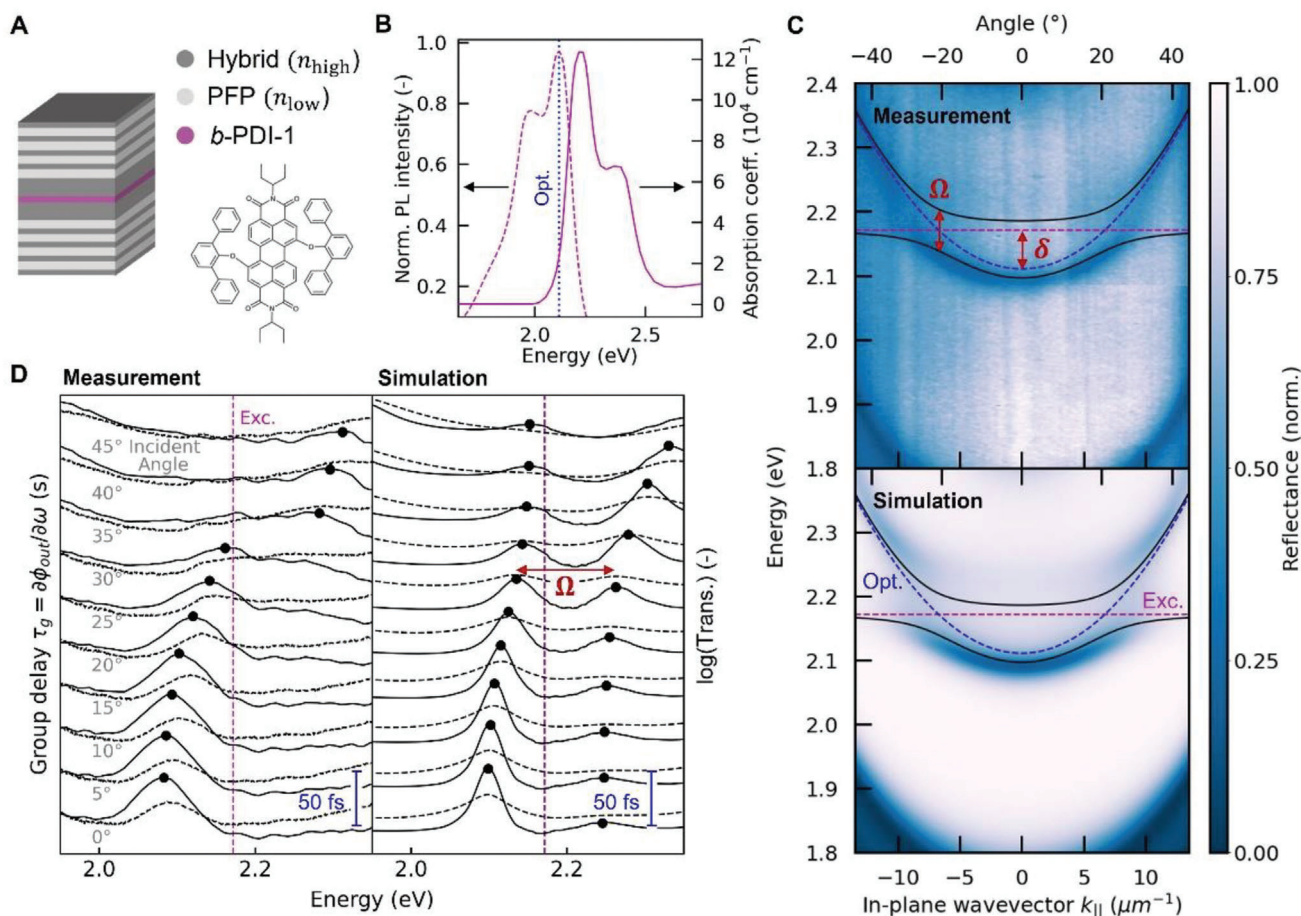
Figure 3. Strong light–matter coupling in a fully solution-processed active *b*-PDI-1 microcavity. A) Microcavity architecture and chemical structure of *b*-PDI-1 used to produce the active organic layer. B) Absorption coefficient and photoluminescence of a 30 nm-thick, active *b*-PDI-1 film. The energy of the microcavity's optical mode (Opt.) at zero angle and in-plane wavevector are indicated with a blue dotted line. C) Energy dispersion relation in reflectance, measured (top) and predicted by the transfer matrix model (bottom), displaying two exciton-polariton states. The observed states agree with those of a Jaynes–Cummings Hamiltonian with a Rabi splitting $\Omega = 2 \times g = 65$ meV (solid black lines), where g corresponds to the Hamiltonian's coupling constant. D) Strong light–matter coupling is also observed in the group delay (solid line) measured via Fourier transform interferometry (left) and simulated using the transfer matrix method (right). Local maxima of the group delay are observed at the upper and lower polariton energies, which correspond with the transmission maxima (dashed lines) at each incident angle.

using Fourier-transform spectral interferometry[40] (data is included in Figure S11 in the Supporting Information), and the group delay was obtained from the numerical differentiation of the measured phase shift. To perform these measurements, the microcavity was placed in one arm of a Mach–Zehnder interferometer, with a non-coated glass substrate as reference in the second arm. The relative phase of the femtosecond pulses in each arm was locked and modulated at a frequency of 14 kHz (see the Section S10, Supporting Information, for more experimental details and a schematic of the setup). Subsequently, the resulting spectral interference pattern was measured with a spectrometer and Fourier-transformed to obtain the phase shift as a function of energy. This experiment was repeated for a series of incident angles.

We start by comparing the microcavity's group delay (solid lines; Figure 3d, left) with its transmission (dashed lines; Figure 3d, left). The transmission maxima correspond to the reflection minima observed in the top panel of Figure 3c and, con-sequently, to the reflection minima observed in the top panel of Figure 3c and, con-sequently, to the energetic positions of the polariton branches. Since the maxima of the group delay at each incident angle (indicated in Figure 3d with solid black circles) match the transmission maxima, we conclude that the group delay as a function of energy and incident angle can represent an alternative way of characterizing the energy dispersion of polaritons in microcavities, providing further evidence of strong light–matter coupling in our fully solution-processed *b*-PDI-1 microcavity. It is important to emphasize that identifying the polariton energies by these means is a direct consequence of their hybrid light–matter nature. The magnitude of the group delay exhibited by these quasi-particles is dominated by their light component and is directly proportional to the photon fraction of each polariton state[39]: the more photon-like a polariton state is, the larger is the group delay exhibited by this polariton state. This result is faithfully reproduced with TMM simulations (Figure 3d, right). (As already noted, the polariton energies in the simulation are slightly higher than those measured experimentally.)

**ADVANCED
SCIENCE NEWS**

www.advancedsciencenews.com

**ADVANCED
MATERIALS**

www.advmat.de

3. Conclusions

Our results demonstrate that high-quality optical microcavities can be reduced entirely from solution. We fabricated planar microcavities based on two DBRs separated by either passive or active spacer layers. Structures with passive spacers exhibited *Q*-factors comparable to those predicted by transfer matrix simulations. Microcavities with active (i.e., absorptive and emissive) spacers displayed strong light–matter coupling, evidenced by measurements of their energy-dispersion relation and group delay. These observations highlight that the use of a novel high-refractive-index molecular hybrid material,[26] employed as the high-refractive-index layer in the DBRs, enables the production of high-quality polymer-based optical microcavities using straightforward coating techniques. All characterization, proceeding the layer-by-layer deposition of the entire cavity stacks, ably demonstrates large refractive-index contrast within the DBR layers without deleterious optical loss. This is in strong contrast to previous work on solution-processed microcavities, where all-polymer bilayers such as polystyrene (PS)/poly(methyl methacrylate) (PMMA),[41] poly(9-vinyl carbazole) (PVK)/poly(acrylic acid),[42] and PS/cellulose acetate[43] were used for the DBR fabrication. These polymers cover a relatively limited refractive-index range and, thus, lead to low refractive-index contrast between DBR layers. While the use of nanocomposites of an inorganic species, such as TiO_2, SiO_2, or CdS nanoparticles blended with a polymer matrix, increases the refractive-index contrast between DBR layers,[44,45] it also typically leads to optical loss and, thus, a reduced microcavity performance. The molecular hybrid employed here circumvents these issues. It is based on a system where the inorganic species coordinates with the organic component, thereby preventing the formation of light-scattering inorganic particles;[26] it also is of amorphous nature enabling fabrication of high-quality films (see Figure S1, Supporting Information). Fully solution-processed optical cavities, as presented here, thus, deliver a versatile "tool" for accurate microcavity design and simple fabrication. In turn, this expands our capabilities for realizing strong light–matter coupling with a broad variety of active materials, making more accessible the light and matter property modifications offered by the strong light–matter coupling regime.

Supporting Information

Supporting Information is available from the Wiley Online Library or from the author.

Acknowledgements

Conflict of Interest

The authors declare no conflict of interest.

Data Availability Statement

The data that support the findings of this study are available from the corresponding author upon reasonable request.

Keywords

[1] C. Weisbuch, M. Nishioka, A. Ishikawa, Y. Arakawa, *Phys. Rev. Lett.* **1992**, *69*, 3314.

[2] D. G. Lidzey, D. D. C. Bradley, M. S. Skolnick, T. Virgili, S. Walker, D. M. Whittaker, *Nature* **1998**, *395*, 53.

[3] B. P. Singh, W. Narazaki, T. Watanabe, Y. Maeda, *Proc. SPIE 1998*, 3211, https://doi.org/10.1117/12.345361.

[4] A. Kavokin, *Phys. Status Solidi B* **2010**, *247*, 1898.

[5] S. Kéna-Cohen, S. A. Maier, D. D. C. Bradley, *Adv. Opt. Mater.* **2013**, *1*, 827.

[6] D. Polak, R. Jayaprakash, T. P. Lyons, L. A. Martinez-Martinez, A. Leventis, K. J. Fallon, H. Coulthard, D. G. Bossanyi, K. Georgiou, A. J. Petty Ii, J. Anthony, H. Bronstein, J. Yuen-Zhou, A. I. Tartakovskii, J. Clark, A. J. Musser, *Chem. Sci.* **2020**, *11*, 343.

[7] D. Ballarini, M. De Giorgi, S. Gambino, G. Lerario, M. Mazzeo, A. Genco, G. Accorsi, C. Giansante, S. Colella, S. D'Agostino, P. Cazzato, D. Sanvitto, G. Gigli, *Adv. Opt. Mater.* **2014**, *2*, 1076.

[8] T. Virgili, D. G. Lidzey, M. Grell, S. Walker, A. Asimakis, D. D. C. Bradley, *Chem. Phys. Lett.* **2001**, *341*, 219.

[9] R. F. Oulton, N. Takada, J. Koe, P. N. Stavrinou, D. D. C. Bradley, *Semicond. Sci. Technol.* **2003**, *18*, S419.

[10] D. G. Lidzey, J. Wenus, D. M. Whittaker, G. Itskos, P. N. Stavrinou, D. D. C. Bradley, R. Murray, *J. Lumin.* **2004**, *110*, 347.

[11] K. S. Daskalakis, S. A. Maier, R. Murray, S. Kena-Cohen, *Nat. Mater.* **2014**, *13*, 271.

[12] D. Snoke, P. Littlewood, *Phys. Today* **2010**, *63*, 42.

[13] K. E. McGhee, A. Putintsev, R. Jayaprakash, K. Georgiou, M. E. O'Kane, R. C. Kilbride, E. J. Cassella, M. Cavazzini, D. A. Sannikov, P. G. Lagoudakis, D. G. Lidzey, *Sci. Rep.* **2021**, *11*, 20879.

[14] K. E. McGhee, R. Jayaprakash, K. Georgiou, S. L. Burg, D. G. Lidzey, *J. Mater. Chem. C* **2022**, *10*, 4187.

[15] J. Ren, Q. Liao, H. Huang, Y. Li, T. Gao, X. Ma, S. Schumacher, J. Yao, S. Bai, H. Fu, *Nano Lett.* **2020**, *20*, 7550.

[16] T. Ishii, K. Miyata, M. Mamada, F. Bencheikh, F. Mathevet, K. Onda, S. Kéna-Cohen, C. Adachi, *Adv. Opt. Mater.* **2021**, 10, 2102034.

[17] T. Cookson, K. Georgiou, A. Zasedatelev, R. T. Grant, T. Virgili, M. Cavazzini, F. Galeotti, C. Clark, N. G. Berloff, D. G. Lidzey, P. G. Lagoudakis, *Adv. Opt. Mater.* **2017**, 5, 1700203.

[18] G. Lerario, A. Fieramosca, F. Barachati, D. Ballarini, K. S. Daskalakis, L. Dominici, M. De Giorgi, S. A. Maier, G. Gigli, S. Kéna-Cohen, D. Sanvitto, *Nat. Phys.* **2017**, 13, 837.

[19] E. R. Bittner, R. A. Malatesta, G. D. Olinger, C. Silva-Acuña, arXiv: 2104.09631, **2021**.

[20] A. Thomas, J. George, A. Shalabney, M. Dryzhakov, S. J. Varma, J. Moran, T. Chervy, X. Zhong, E. Devaux, C. Genet, J. A. Hutchison, T. W. Ebbesen, *Angew. Chem., Int. Ed.* **2016**, 55, 11462.

[21] A. Kavokin, J. Baumberg, G. Malpuech, F. Laussy, *Microcavities*, Oxford University Press, Oxford, New York **2017**.

[22] R. P. Sabatini, F. Maasoumi, S. K. K. Prasad, B. Zhang, C. Clark, T. W. Schmidt, W. W. H. Wong, G. Lakhwani, *Appl. Phys. Lett.* **2020**, 117, 041103.

[23] S. Kéna-Cohen, M. Davanco, S. R. Forrest, *Phys. Rev. Lett.* **2008**, 101, 116401.

[24] S. Kéna-Cohen, S. R. Forrest, *Nat. Photonics* **2010**, 4, 371.

[25] M. G. Ramírez, S. Pla, P. G. Boj, J. M. Villalvilla, J. A. Quintana, M. A. Díaz-García, F. Fernández-Lázaro, Á. Sastre-Santos, *Adv. Opt. Mater.* **2013**, 1, 933.

[26] M. Russo, M. Campoy-Quiles, P. Lacharmoise, T. A. M. Ferenczi, M. Garriga, W. R. Caseri, N. Stingelin, *J. Polym. Sci., Part B: Polym. Phys.* **2012**, 50, 65.

[27] S. Bachevillier, H. K. Yuan, A. Strang, A. Levitsky, G. L. Frey, A. Hafner, D. D. C. Bradley, P. N. Stavrinou, N. Stingelin, *Adv. Funct. Mater.* **2019**, 29, 1808152.

[28] S. Bachevillier, H. K. Yuan, K. Tetzner, D. D. C. Bradley, T. D. Anthopoulos, P. N. Stavrinou, N. Stingelin, *Mater. Horiz.* **2022**, 9, 411.

[29] H. A. MacLeod, *Thin-Film Optical Filters*, CRC Press, Boca Raton, FL, USA **2010**.

[30] S. D. Smith, *J. Opt. Soc. Am.* **1958**, 48, 43.

[31] M. Slootsky, Y. Zhang, S. R. Forrest, *Phys. Rev. B* **2012**, 86, 045312.

[32] D. Sannikov, T. Yagafarov, K. Georgiou, A. Zasedatelev, A. Baranikov, L. Gai, Z. Shen, D. Lidzey, P. Lagoudakis, *Adv. Opt. Mater.* **2019**, 7, 1900163.

[33] M. Wei, S. K. Rajendran, H. Ohadi, L. Tropf, M. C. Gather, G. A. Turnbull, I. D. W. Samuel, *Optica* **2019**, 6, 1124.

[34] S. Betzold, M. Dusel, O. Kyriienko, C. P. Dietrich, S. Klembt, J. Ohmer, U. Fischer, I. A. Shelykh, C. Schneider, S. Höfling, *ACS Photonics* **2019**, 7, 384.

[35] J. Mony, M. Hertzog, K. Kushwaha, K. Borjesson, *J. Phys. Chem. C* **2018**, 122, 24917.

[36] G. Zheng, R. Horstmeyer, C. Yang, *Nat. Photonics* **2013**, 7, 739.

[37] E. T. Jaynes, F. W. Cummings, *Proc. IEEE Inst. Electr. Electron Eng.* **1963**, 51, 89.

[38] F. W. Cummings, *Phys. Rev.* **1965**, 140, A1051.

[39] J. M. Bendickson, J. P. Dowling, M. Scalora, *Phys. Rev. E* **1996**, 53, 4107.

[40] L. Lepetit, G. Chériaux, M. Joffre, *J. Opt. Soc. Am. B* **1995**, 12, 2467.

[41] W. Mönch, J. Dehnert, O. Prucker, J. Rühe, H. Zappe, *Appl. Opt.* **2006**, 45, 4284.

[42] N. Valappil, M. Luberto, V. M. Menon, I. Zeylikovich, T. K. Gayen, J. Franco, B. B. Das, R. R. Alfano, *Photonics Nanostruct.* **2007**, 5, 184.

[43] L. Frezza, M. Patrini, M. Liscidini, D. Comoretto, *J. Phys. Chem. C* **2011**, 115, 19939.

[44] P. K. H. Ho, D. D. Thomas, R. H. Friend, N. Tessler, *Science* **1999**, 285, 233.

[45] L. A. DeSilva, R. Gadipalli, A. Donato, T. M. W. J. Bandara, *Optik* **2018**, 157, 360.